# Fixed-bed adsorption of toluene on high silica zeolites: experiments and mathematical modelling using LDF approximation and a multisite model

Nicolas Brodu, Sabine Sochard, Caroline Andriantsiferana, Jean-Stéphane Pic, Marie-Hélène Manero

# Fixed-bed adsorption of toluene on high silica zeolites: experiments and mathematical modelling using LDF approximation and a multisite model

Nicolas Brodu[a,b*], Sabine Sochard[c], Caroline Andriantsiferana[a,b], Jean-Stéphane Pic[d] and Marie-Hélène Manero[a,b]

*[a]INPT, UPS, Laboratoire de Génie Chimique, Université de Toulouse, 4, Allée Emile Monso, F-31030 Toulouse, France; [b]CNRS, Laboratoire de Génie Chimique, F-31030 Toulouse, France; [c]Laboratoire de Thermique Energétique et Procédés, Université de Pau et des Pays de l'Adour, ENSGTI, rue Jules Ferry, BP 7511, 64075 Pau Cedex, France; [d]Laboratoire d'Ingénierie des Systèmes Biologiques et des Procédés, UMR INSA/CNRS 5504 & UMR INSA/INRA 792, Université de Toulouse, 135 Avenue de Rangueil, 31077 Toulouse Cedex 4, France*

The adsorption of toluene (TOL) as a target volatile organic compound has been studied experimentally and modelled on various hydrophobic zeolites: Faujasite (FAU), ZSM-5 (Z) and Mordenite (MOR). The influence of the nature of the compensating cation ($H^+$ or $Na^+$) has also been investigated for ZSM-5 zeolite, which is known to possess three kinds of adsorption sites (sinusoidal channels, straight channels and intersections). Type I isotherms observed on FAU, Na-Z and MOR fitted well with the Langmuir model. A deviation from a type I isotherm was observed for H-Z, because of the structure of this zeolite. The Successive Langmuir Model was more successful to fit the 'bump' of the experimental curve than the Double Langmuir. Classical shapes were found for MOR, FAU and Na-Z breakthrough curves that were fitted with good accuracy using the Linear Driving Force (LDF) approximation. In the case of H-Z, a change of profile was observed during the dynamic adsorption and the differences seen between the Na-Z and H-Z behaviours were explained by the strong interactions between $Na^+$ and adsorbed TOL at the intersection sites. The $Na^+$ cations prevented reorientation of TOL molecules at the intersection and thereby avoided the filling of the sinusoidal channel segments. Thus, a specific model was developed for fitting the breakthrough curve of H-Z. The model developed took into account these two types of adsorption sites with the overall uptake for each site being given by an LDF approximation.

**Keywords:** volatile organic compounds; adsorption; breakthrough curve modelling; hydrophobic zeolite; compensating cation

## 1. Introduction

Volatile organic compounds (VOCs) are used extensively in many industrial processes. The main anthropogenic sources of emissions of VOCs are oil and gas refineries, and the surface treatment or the evaporative emissions due to the use of solvents.[1,2] Emissions of VOCs are responsible for different problems of indoor and outdoor air pollution [3] that may affect human health, as many of these compounds are toxic or even carcinogenic.[4] They have also been identified as playing a major role in serious environmental problems such as the photochemical smog that can cause damage to both humans and the environment.[5–7] Therefore, the removal of VOCs is of significant importance in air quality control and has triggered the interest in the development of abatement technologies to comply with the latest environmental regulations.

The usual way to reduce the harmful effects of VOCs is to reduce their concentration. Many processes are used in industry for controlling environmental pollution such as adsorption and catalytic oxidation.[8–10] Nowadays among the treatments used for reducing VOCs, adsorption technology appears to be the best strategy as it removes pollutants economically in terms of simplicity of design, ease of operation and low energy requirements.[11–13] Adsorption has also been found to be effective at low concentration levels.[14]

The success of an adsorption process depends on the performance of adsorbents in terms of both equilibria and kinetics: a solid support that has a favourable adsorption isotherm as well as rapid kinetics is the ideal. Several adsorbents have been extensively studied for VOC removal from air streams, such as silica gel, zeolites, mesoporous materials and activated carbons. Activated carbon is the most widely used adsorbent thanks to its high surface area, pore structure [15,16] and low price.[17] However, there is increasing interest in developing new adsorbents as an alternative to activated carbon because of its humidity dependence [18] and the difficulty in regenerating it.[19] The use of hydrophobic zeolites is interesting because it is reported that these materials have chemical and thermal stability, are not flammable and retain good adsorption

*Corresponding author. Email: nicolas.brodu@gmail.com

capacities at relatively high humidity.[17] Moreover, they can easily be regenerated.[9]

Zeolites are crystalline aluminosilicates with unique microporosity properties. The crystalline framework structure, high specific area and their structural and compositional flexibility make zeolites potential candidates for VOC adsorption.[11,18] Adsorption on zeolite has been reported to depend on the adsorbent crystalline framework, pore structure, compensating cation and chemical properties.[20]

Numerous models have been published to describe the phenomena taking place in fixed-bed adsorption. Indeed, adsorption is composed of several steps: mass transfer in the boundary layer surrounding the adsorbent particles (external transfer), diffusion inside the pores (internal transfer), adsorption onto the pore walls and surface diffusion along the internal pore surface. The drawback of sophisticated models taking both external and internal transfer into account is that they require the determination of a large number of parameters and that they are difficult to solve numerically.[21,22] Therefore, in most studies, the adsorption process is modelled using simplistic mathematical expressions allowing significant savings in computation time. The most simplistic approach is to assume equilibrium, and to neglect resistance to mass transfer [23]; obviously, this approach can be only used in certain conditions or to obtain an order of magnitude of the adsorption parameters. The Thomas model, which is a lumped parameter model, can give good results.[24,25] In this model, a pseudo adsorption kinetic coefficient is determined by fitting the calculated breakthrough curve to experimental data. This parameter includes external and internal transfer as well as adsorption kinetics. Another well-known simple model is the Linear Driving Force (LDF) approximation [15,26–28]: the mass balance equation within the particle is replaced by an expression giving the overall uptake rate in the particle. This adsorption rate is assumed to be linearly proportional to a driving force defined as the difference between the surface concentration and the average adsorbed-phase concentration. Several authors have proposed a relationship linking the global transfer coefficient $k_p$ to the effective intrapellet diffusivity. Tien [28] noticed that although this relationship has been obtained on a theoretical basis, $k_p$ should above all be considered as an adjustable parameter in modelling adsorption calculations. However, all these models assume only one single type of adsorption site and dynamic models that consider adsorption in multi-compartment porous media are rare.[29,30] Lesage et al. [29] assumed that the different types of pores are parallel, while Ding et al. [30] proposed a model where the two types of pores are interconnected, leading to a complex numerical resolution.

Our current research encompasses the development of a process combining VOC adsorption and catalytic ozonation on hydrophobic zeolites. The study presented here focused on the adsorption, 'that is, the first step of this combined process, and its aims were: (i) to investigate the effects of zeolite channel size and pore structure on the adsorption using three commercial hydrophobic zeolites: mordenite (MOR), ZSM-5 and faujasite (FAU); (ii) to analyse the effect of the compensating cation and (iii) to obtain and model the breakthrough curves for toluene (TOL). For these purposes, gas–solid equilibrium experiments and dynamic adsorption experiments were carried out. The breakthrough curves obtained by dynamic adsorption were compared to the theoretical prediction of the models. The influence of the pore structure of the zeolites on mass transfer was studied to understand the adsorption mechanism. In this study, two models are used: the LDF model and a two-adsorption sites model that was specially developed for this work.

## 2. Materials and methods

### 2.1. *Adsorbents*

Four kinds of hydrophobic microporous zeolites were used as adsorbents: MOR, FAU and two ZSM-5 (Z). For the latter, the nature of the compensating cation is different: $Na^+$ and $H^+$. The schemes of the structure of these three zeolites are shown in Figure 1. Mordenite type zeolites consist mainly of 12-membered straight channels and apertures of 6.5 × 7 Å with the presence of side pockets (2.6 × 5.7 Å). FAU-type zeolites consist of cubic-octahedrons called sodalite cages or $\beta$-cages.[31] The assembly of $\beta$-cages linked together by hexagonal prisms gives 13 Å diameter supercages interconnected by 12 oxygen atom apertures (7.4 Å diameter). ZSM-5 zeolite has a three-dimensional pore network with 10-membered straight and sinusoidal ring channels and apertures of 5.3 × 5.6 Å and 5.1 × 5.5 Å, respectively.

The four zeolites were provided by Tosoh and Zeochem. Zeolite pellets consist of microcrystals fixed together as cylindrical pellets with a binder (clay, alumina), creating a meso/macroporous structure. A thermal degassing procedure was applied prior to the experiments. The zeolite samples were oven-dried at 500°C for 6 h, and stored in desiccators until further use.

### 2.2. *Characterization of zeolite samples*

Specific surface areas and pore volumes were obtained by nitrogen adsorption–desorption at −196°C using a Micromeritics ASAP 2010 instrument. Prior to nitrogen adsorption, the zeolite samples were degassed at 90°C for 1 h and then at 350°C for 4 h. Specific surface areas ($S_{BET}$) were calculated from nitrogen adsorption isotherms, using the Brunauer–Emmett–Teller (BET) equation.[32] Micropore volumes ($V_{micro}$) were determined by applying the Horvath–Kawazoe method.[33] Table 1 summarizes the physicochemical characteristics of the zeolite samples. Samples are named according to the compensating cation

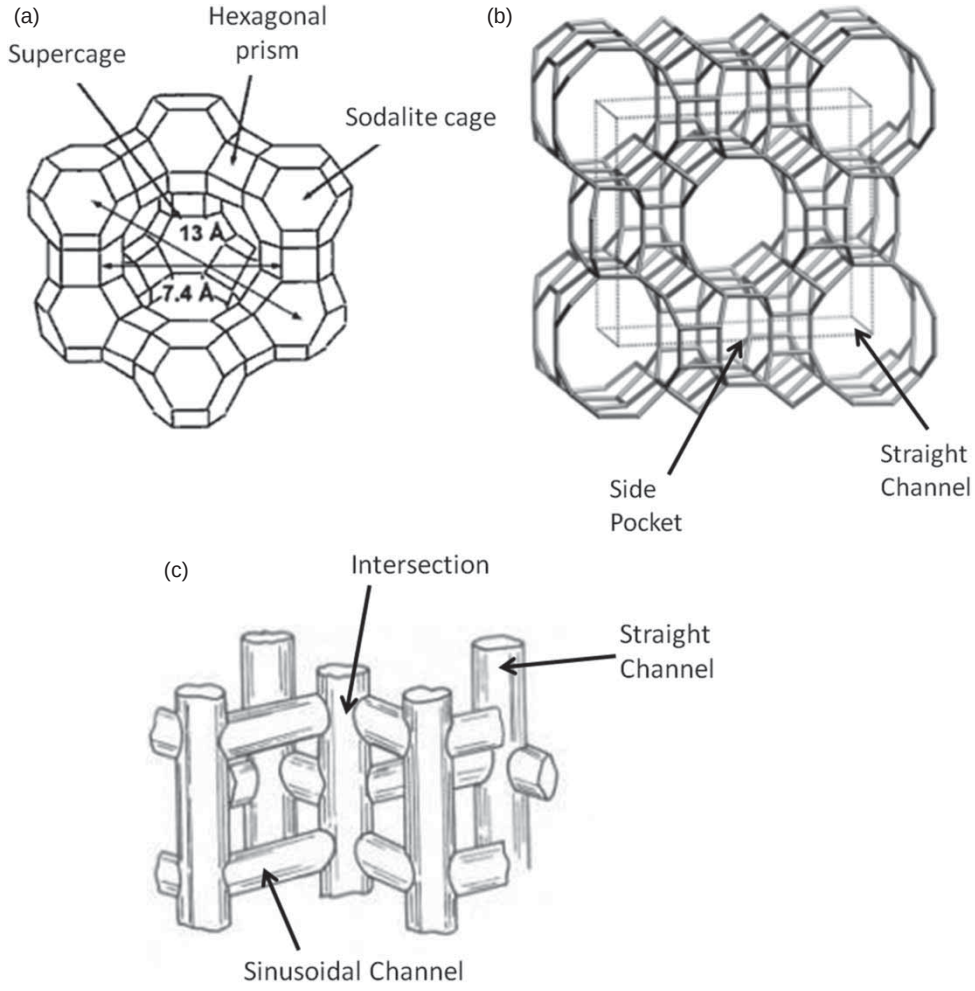


Figure 1. Zeolite structure: MOR (a), FAU (b), ZSM-5 (c).

Table 1. Physical–chemical properties of the zeolites.

| Sample | Zeolite | Compensating cation | Pore size aperture (Å) | $d_p$[a] (mm) | Binder weight (%) | a[b] ($m^2$ $m^{-3}$) | $S_{BET}$ ($m^2$ $g^{-1}$) | $V_{micro}$ ($cm^3$ $g^{-1}$) | Si/$Al_2$ ratio[c] |
|---|---|---|---|---|---|---|---|---|---|
| Na-Z | ZSM-5 | $Na^+$ | 5.1 × 5.5<br>5.3 × 5.6 | 1.7 | / | 3529 | 309 | 0.12 | 360 |
| H-Z | ZSM-5 | $H^+$ | 5.1 × 5.5<br>5.3 × 5.6 | 1.6 | 20 | 3750 | 308 | 0.11 | 2100 |
| H-FAU | FAU | $H^+$ | 7.4 | 1.8 | 20 | 3333 | 608 | 0.23 | 13.8 |
| H-MOR | MOR | $H^+$ | 2.6 × 5.7 (pocket)<br>6.5 × 7 (channel) | 1.8 | 20 | 3333 | 508 | 0.21 | 230 |

Note: / – Not given by the provider.
[a]Equivalent spherical particle diameter of the cylindric pellets: $V_{pellets}/S_{pellets.}$
[b]Equivalent spherical specific area ($6/d_p$).
[c]Given by the provider.

and the name of the zeolite. As it can be seen, the physical properties of H-Z and Na-Z are similar although the Si/$Al_2$ ratio and the nature of the compensating cation are different.

### *2.3. Adsorbate / Analytical procedure*

TOL was used as a model VOC (Sigma-Aldrich, purity more than 99%). The kinetic diameter of this molecule is 5.8 Å.[16]

The concentration of TOL was analysed using a GAS chromatograph Varian 3800 GC equipped with Flame Ionization Detectors. Separation was achieved using a CP-SIL 8 capillary column (30 m × 0.53 mm ID) with a 1.0 µm film thickness.

### 2.4. Adsorption isotherms

Adsorption isotherms were determined at 25°C (±1°C) using a volumetric method detailed in a previous publication.[15] All the points were obtained in triplicate. The adsorbed quantity ($Q_e$) was calculated from a mass balance in the gas phase:

$$Q_e = \frac{V}{m}(C_o - C_e), \quad (1)$$

where $C_o$ and $C_e$ are the initial and equilibrium concentrations (mol $m^{-3}$), respectively , $V$ is the volume of the reactor ($m^3$) and $m$ is the mass of solid (kg).

### 2.5. Experimental breakthrough curves

The experimental set-up used is shown in Figure 2. Dynamic adsorption experiments were conducted in a fixed-bed flow reactor (4.5 cm ID; length 15 cm), at 21°C (±1°C) and 101 kPa. The dry air/VOC mixture was generated using a bubbling system and diluted by adding dry air. The flow rate was fixed at 1.83 $m^3$ $h^{-1}$ and the VOC concentration was fixed at 0.011 mol $m^{-3}$. The VOC concentrations at the inlet and at the outlet of the reactor were analysed on-line.

The experimental conditions are summarized in Table 2. Total adsorbed TOL $Q$ (mol $kg^{-1}$) was calculated from a mass balance using the following equation:

$$Q = \frac{FC_{TOLin}}{m}\int_0^{t_s}\left(1 - \frac{C}{C_{TOLin}}\right)dt, \quad (2)$$

where $C_{TOLin}$ is the inlet concentration of TOL (mol $m^{-3}$); $F$ is the volumetric flow rate ($m^3$ $h^{-1}$) and $t_s$ is the time needed to reach zeolite saturation (h); $C$ is the outlet TOL concentration as function of time (mol $m^{-3}$).

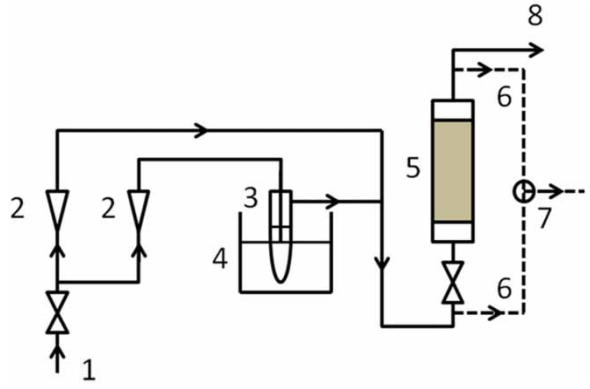


Figure 2. Experimental set-up for dynamic adsorption. (1) Dry air inlet; (2) flowmeter; (3) bubbler; (4) thermostated tank; (5) adsorption bed; (6) gas sample outlet; (7) three-way valve to gas analyser; (8) exhaust gas.

Table 2. Experimental conditions used to carry out the breakthrough curves.

| Sample | $H$ (m) | $m$ (g) | $\rho$ (kg $m^{-3}$) | $\epsilon$ (-) |
|---|---|---|---|---|
| Na-Z | 0.09 | 132 | 845 | 0.36 |
| H-Z | 0.09 | 98 | 680 | 0.39 |
| H-FAU | 0.09 | 70 | 490 | 0.35 |
| H-MOR | 0.09 | 91 | 658 | 0.34 |

Note: With $H$, $m$, $\rho$, $\epsilon$ being the length, the mass, the density and the void fraction of the fixed-bed of zeolite pellets.

## 3. Results and discussions

### 3.1. Isotherms

The adsorption isotherms of TOL are shown in Figure 3. It can be noted that the H-FAU, H-MOR and Na-Z curves are type I isotherms. A higher adsorption capacity can be observed for H-FAU than for H-MOR and for Na-Z, probably due to a higher specific surface area ($S_{BET}$) for H-FAU than for H-MOR and for Na-Z as shown on Table 1. However, in the case of zeolites, the value of $S_{BET}$ is not the only important parameter since the kinetic diameters of the pollutants are often of the same order of magnitude than the pore aperture. In the present study, it can be noted that H-FAU possesses larger pore aperture, avoiding steric hindrance. Although the micropore volume of H-MOR is similar to H-FAU, the side pocket (2.6 × 5.7 Å) is not accessible to the molecules of TOL (5.8 Å) and the available adsorption volume is then reduced by 53%.[31] The usual Langmuir model gives a very good representation of the experimental H-FAU, Na-Z and H-MOR isotherms as expected for type I isotherms.

However, the Langmuir model does not fit well with the experimental adsorption isotherm of H-Z, as shown in Figure 3(b). In fact, the isotherm of H-Z shows two steps: the first step is observed for $Q_e$ around 0.6 mol $kg^{-1}$; then, a second step seems to start when $C_e$ is superior to 0.051 mol $m^{-3}$. This leads to a higher capacity for H-Z than for Na-Z although its specific surface is the same than Na-Z. S-shaped isotherms usually describe multilayer adsorption. However, the kinetic diameter of TOL (5.8 Å) is of the same order of magnitude than the pore aperture so that a second layer is not possible. A similar isotherm profile has been reported in the case of the adsorption isotherm of aromatic compounds over silicalite-1 zeolite by Song et al.[34]. The authors clearly pointed that this behaviour is not due to multilayer adsorption but it is suggested that two sites of adsorption are active for H-Z: the intersections and the channels. Therefore, two different variations of Langmuir models can be used: the Double Langmuir (DL) model and the Successive Langmuir (SL) model. Both

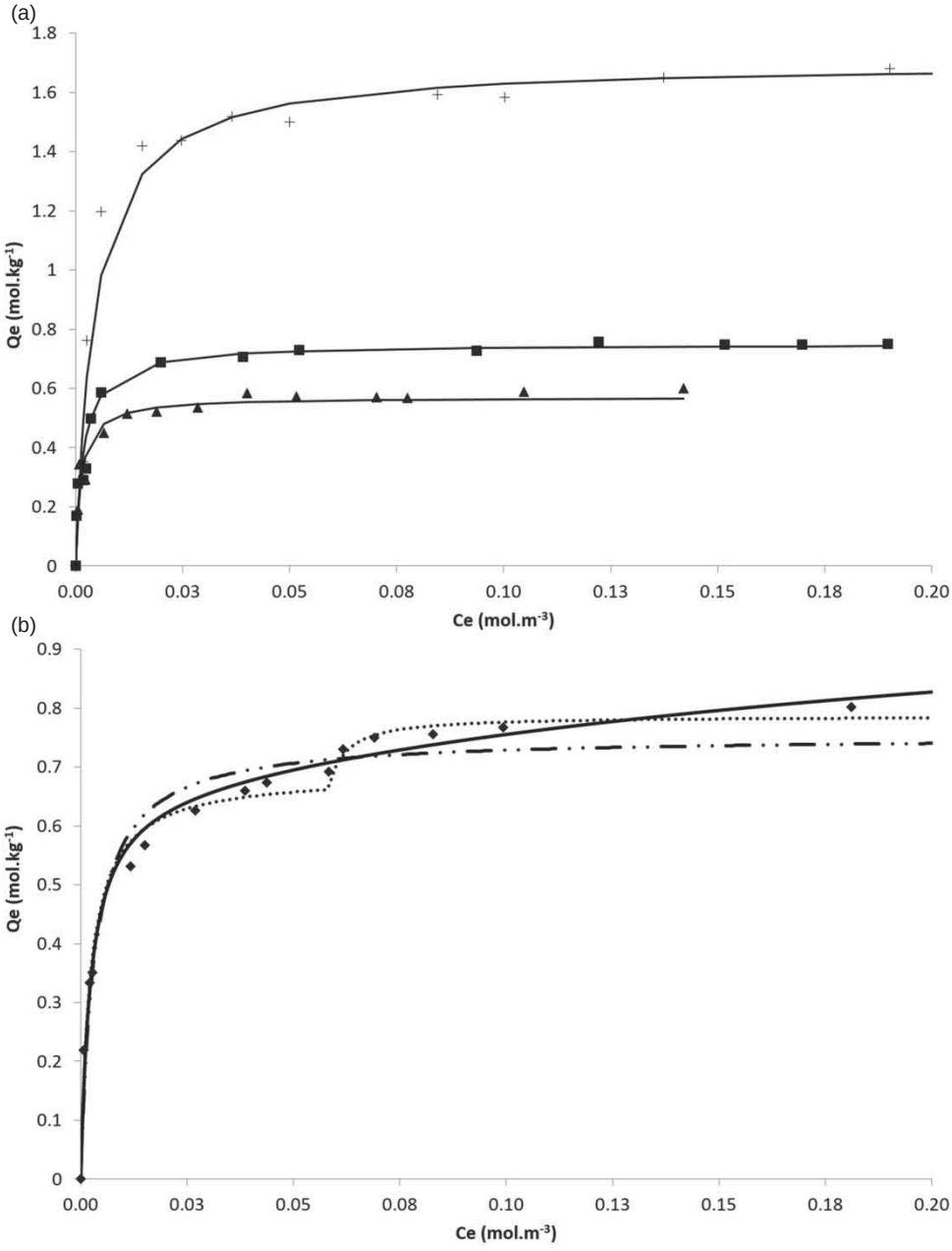


Figure 3. (a) Adsorption isotherm of zeolites at 25°C and 101 kPa: (▲) Na-Z; (■) H-MOR; (+) H-FAU; (–) simulated with Langmuir model. (b) Adsorption isotherm of zeolites at 25°C and 101 kPa: (♦) H-Z; (—··) simulated with Langmuir model; (···) simulated with two successive Langmuir models; (–) simulated with Double Langmuir model.

consider two sites of adsorption, but not with the same assumptions. The DL model describes a simultaneous filling of the two adsorption sites (just like heterogeneous surface with many adsorption sites [28]) whereas the SL model considers a successive filling of the two adsorption sites. The equations can be read in Table 3 and the results of the modelling can be seen in Figure 3(b). It can be shown that both the models give a good accuracy for the first part of the curve. As suggested by Wang et al.[35], low-loading adsorptions take place at the energetically preferred site and thus, for low loadings, the DL model is as accurate as the SL model. This is not the case for higher loadings. Despite the high degree of accuracy with the experimental data, compared to a simple Langmuir model, the DL model does not represent the second step very well. This is probably due to the fact that this model describes a filling up of both sites at the same time (just like for a heterogeneous surface). The better result obtained by the SL model seems to show that the two sites do not fill up at the same time. It can be supposed that the intersections are the preferential adsorption site of the zeolite H-Z and in the case of high loadings, and after the complete loading of the TOL

Table 3. Identified parameters fitting Langmuir, DL or SL models to the experimental isotherm data.

| | Isotherm model | $Q_{max}$ (mol kg$^{-1}$) | b (m$^3$ mol$^{-1}$) |
|---|---|---|---|
| H-MOR | Langmuir[a] | 0.75 | 552 |
| H-FAU | Langmuir | 1.70 | 227 |
| Na-Z | Langmuir | 0.57 | 810 |
| H-Z | Langmuir | 0.75 | 309 |
| | Successive Langmuir[b] | 0.69/0.12 | 426/264 |
| | Double Langmuir[c] | 0.66/0.43 | 437/3.35 |

Note: $b_i$, $Q_{maxi}$, $b_c$, $Q_{maxc}$ are the parameters of the Successive Langmuir model or DL model with subscripts i and c denoting the intersections and channels, respectively.

[a] $Q_e = \frac{b\ Q_{max}\ C_e}{1+b\ C_e}$.

[b] $Q_e = \frac{b_i\ Q_{maxi}\ C_e}{1+b_i\ C_e}$ if $C_e \le C_{lim} = 0.051$ mol m$^{-3}$,
$Q_e = \frac{b_i\ Q_{maxi}\ C_{lim}}{1+b_i\ C_{lim}} + \frac{b_c\ Q_{maxc}\ (C_e - C_{lim})}{1+b_c(C_e - C_{lim})}$ if $C_e > C_{lim}$.

[c] $Q_e = \frac{b_i\ Q_{maxi}\ C_e}{1+b_i\ C_e} + \frac{b_c\ Q_{maxc}\ C_e}{1+b_c\ C_e}$.

molecules on these sites, the adsorption goes on inside the sinusoidal channels. This assumption is reinforced by the fact that the second step appears when four molecules per unit cell is sorbed corresponding to the number of the intersections per unit cell.[34] Song et al [34] suggested that there is redistribution and/or reorientation of molecules sorbed in the framework when the sorbed molecules start to populate the sinusoidal channels. Hence, we suggest that some of the molecules sorbed on the intersections can migrate to the sinusoidal channels, so that new molecules can again be adsorbed at the intersections. Then the two SL models seem to be more adapted to fit the isotherm of TOL on H-Z.

The identified values of the parameters of the models are given in Table 3. In the cases of the DL model and of the SL model, it should be noted that the value of $Q_{maxi}$ (0.66 or 0.69 mol kg$^{-1}$) is close to the value corresponding to a loading of four molecules per unit cell (0.56 mol kg$^{-1}$). Moreover, $b_i$ is greater than $b_c$, indicating that the adsorption at the intersections is easier than the adsorption in the channels. Indeed, at low loadings, the TOL molecules only move along the straight channels up to the intersections. However, they have to reorient at the level of the intersections in order to populate the sinusoidal channels [34,36] because of the strong adsorbate–adsorbate interactions, leading to a lower coefficient $b_c$.

These results are consistent with other studies.[18,34] The difference between the Na-Z and H-Z isotherms is probably related to the nature of compensating cation. A steric hindrance can be induced by the larger size of $Na^+$ (1.16 Å) compared to the diameter of $H^+$ ($1.6.10^{-5}$ Å). Since the kinetic diameter of TOL and the dimensions of the sinusoidal channels are 5.8 Å and 5.1 × 5.5 Å, respectively, $Na^+$ can block the entry of the sinusoidal channels. The strength of the interaction between the cation and TOL can be another explanation. Indeed, the cation $Na^+$ acts as a Lewis acid to form a strong interaction with $\pi$ electrons in the case of TOL adsorption.[37] The interaction between $Na^+$ and TOL is greater than that between $H^+$ and TOL. This characteristic may affect the adsorption of the hydrocarbon on ZSM-5. Indeed, as explained by Song et al., [34] the strong adsorbate–adsorbate interactions for aromatic adsorbates leads to redistribution and/or reorientation of the molecules adsorbed in the framework when the adsorbed molecules start to populate the channel segments. Thus, we can postulate that, in the case of Na-Z, the reorientation of TOL is not possible due to stronger interactions between $Na^+$ and TOL and thus TOL cannot enter the sinusoidal channels. Therefore the adsorption cannot continue inside the channels and is probably limited to the intersections for Na-Z, contrary to H-Z.

### 3.2. *Breakthrough curves*

Figure 4(a) and 4(b) shows the breakthrough curves of TOL for the different zeolites. The H-MOR gives a better breakthrough curve with a longer breakthrough time and a steeper slope than the other zeolites. The mass transfer of TOL into the pores of MOR is favoured compared to the other zeolites. The breakthrough of H-FAU appears earlier but the slope of the curve is more extended, leading to a later complete loading. Despite the similar physical properties of ZSM-5, the appearance of the breakthrough curve is different between Na-Z and H-Z as was observed for the adsorption isotherms. A change of slope is observed in the course of the breakthrough curve for H-Z whereas a classical shape is observed for Na-Z. This can be due to the strong interaction between the adsorbed molecules [38] and to the presence of two sites of adsorption for the H-Z as mentioned earlier.

#### 3.2.1. *Modelling*

According to the previous results, two models were developed. One kind of site is considered in the first model whereas the second model considers two kinds of adsorption sites. The following assumptions are used for both the models: (i) the pressure drop is negligible; (ii) the system is isothermal for low concentrations; (iii) the plug flow is assumed and the effect of the axial dispersion is considered; (iv) the volumetric flow rate is constant; (v) the adsorbent particles are spherical. In the gas phase, an external film around the particle is postulated. The second model assumes that TOL uptake at the i-sites and c-sites occurs simultaneously. This assumption is consistent with the DL model. However, this second model will be used with the SL model with an adaptation which will be discussed later.

*3.2.1.1. Model with one adsorption site* According to the hypotheses stated earlier, the dynamic adsorption

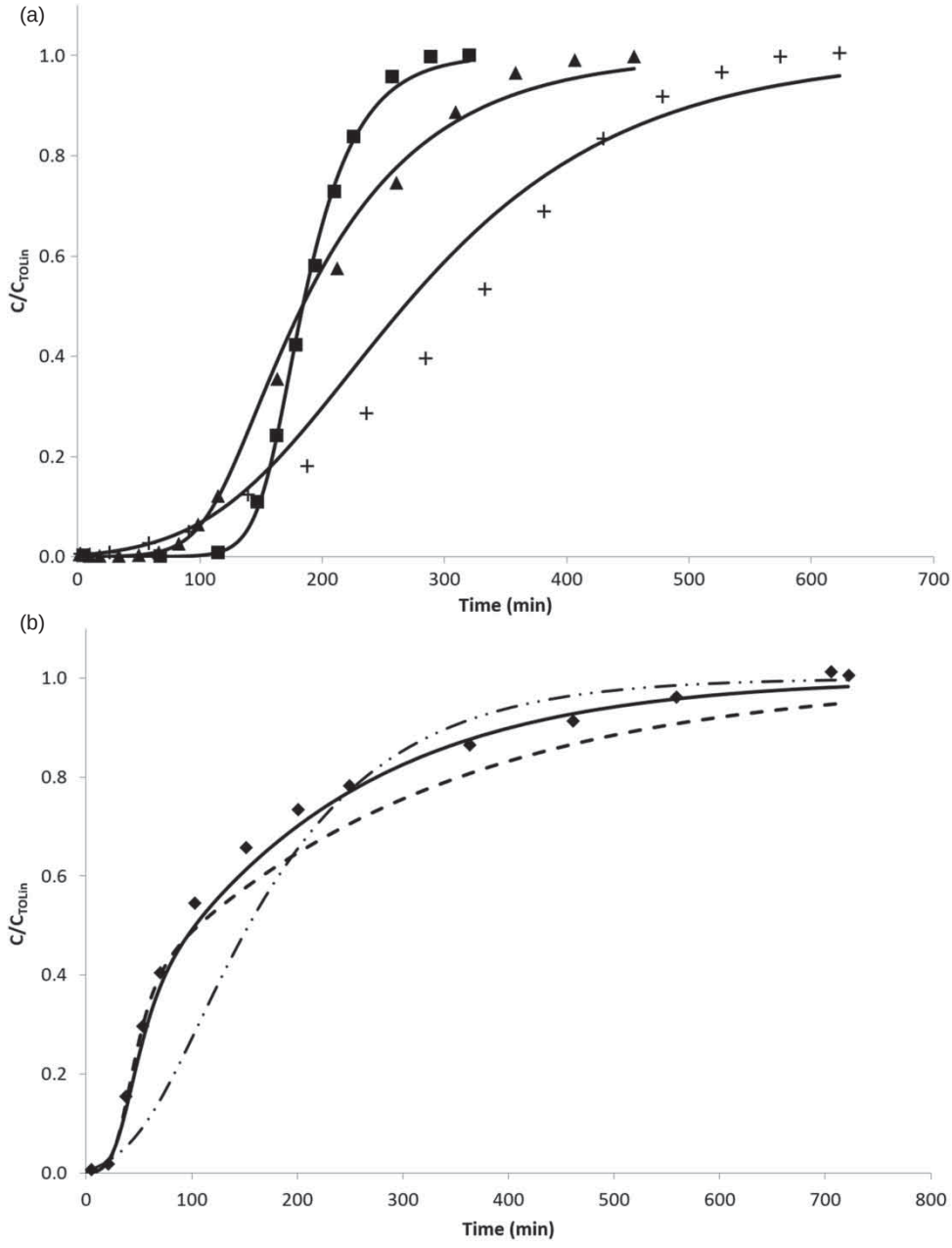


Figure 4. (a): Influence of zeolites on TOL breakthrough: (▲) Na-Z; (■) H-MOR; (+) H-FAU; (—) simulated with Model-1. (b) TOL breakthrough curve on H-Z: (♦) Experimental data; (– ··) adsorption on the two sites using the parameter of the Double Langmuir; (– – –) adsorption on the two sites using the parameter of the Successive Langmuir model; (—) adsorption using $Q_{maxi}$ and $Q_{maxc}$ of the Successive Langmuir model but identifying $b_i$ and $b_c$ to compensate for the lack of the interconnection of the two sites. Operating conditions: 21°C, 101 kPa, $C_{TOLin}$: 0.01 mol m$^{-3}$.

model consists of the following equations.

$$\frac{\partial C}{\partial t} = -\frac{u}{\varepsilon}\frac{\partial C}{\partial z} + D_{ax}\frac{\partial^2 C}{\partial z^2} - \frac{\rho}{\epsilon}\frac{\partial \bar{Q}}{\partial t}, \tag{3}$$

with the boundary conditions:

$$z = 0, \quad \frac{D_{ax}}{u}\frac{\partial C}{\partial z} = C - C_{TOLin}, \tag{4}$$

$$z = H, \quad \frac{\partial C}{\partial z} = 0. \tag{5}$$

$\bar{Q}$ is the mean quantity adsorbed and its derivative is given by the following LDF approximation [15] where $k_p$ is the internal mass transfer coefficient taking into account inter and intracrystalline diffusion (i.e. diffusion through the binder and surface diffusion into the crystals).

$$\frac{\partial \bar{Q}}{\partial t} = k_p(Q_s - \bar{Q}). \tag{6}$$

At the surface of the particle, the concentration of adsorbate in the solid phase $Q_s$ is linked to the

concentration in the gas phase, $C_s$ by the Langmuir equation (Table 3).

The equality of flux through the surface leads to the following equation:

$$k_c a(C - C_s) = \frac{\rho k_p}{(1-\epsilon)}(Q_s - \bar{Q}), \tag{7}$$

where $k_c$ is the external mass transfer coefficient. It can be determined by the semi-empirical equation of Wakao and Funazkri (1978).[39]

The initial conditions of the system were:

$$z \geq 0, \quad \bar{q} = 0, \tag{8}$$

$$z = 0, \quad C = C_{TOLin}, \tag{9}$$

$$z > 0, \quad C = 0. \tag{10}$$

*3.2.1.2. Model with two adsorption sites* Two kinds of sites are considered with their transport features. Thus, two terms of consumption are present ($\partial\overline{Q_i}/\partial t$ and $\partial\overline{Q_c}/\partial t$). The first and second adsorption sites are respectively the intersections and the channels. According to the hypotheses stated earlier, the dynamic adsorption model consists of the following equations:

• Mass balance in the fixed-bed is given by the following equation:

$$\frac{\partial C}{\partial t} = -\frac{u}{\varepsilon}\frac{\partial C}{\partial z} + D_{ax}\frac{\partial^2 C}{\partial z^2} - \frac{\rho}{\epsilon}\left(\frac{\partial\overline{Q_i}}{\partial t} + \frac{\partial\overline{Q_c}}{\partial t}\right). \tag{11}$$

• For each site, a system of equations similar to those of the first model is used.

$$\frac{\partial\overline{Q_x}}{\partial t} = k_{px}(Q_{sx} - \overline{Q_x}) \tag{12}$$

$k_{px}$ is the internal mass transfer coefficient for the site $x$ ($x$ being i for the intersections and c for the channels).

$$k_c a(C - C_{sx}) = \frac{\rho k_{px}}{(1-\epsilon)}(Q_{sx} - \overline{Q_x}), \tag{13}$$

$$Q_{sx} = \frac{b_x\, Q_{maxx}\, C_{sx}}{1 + b_x\, C_{sx}}. \tag{14}$$

For both the sites, $k_c$ is the same external mass transfer coefficient. As already mentioned, $k_c$ is determined by the correlation of Wakao and Funazkri.[39] Yang has pointed out that this correlation should be used when axial dispersion is included in modelling fixed-bed adsorbers and that other correlations have to be used if the dispersion is neglected.[40] In order to estimate the axial dispersion coefficient $D_{ax}$, several correlations exist and give a wide range of values for each zeolite. However, Tien [28] has pointed out that some of these correlations (like the well-known correlation of Edwards and Richardson) have only limited accuracy if the particulate diameter is lower than 3 mm (that is the case for the four zeolites selected in this study), because in this case the limiting value of the Peclet number Pe can deviate significantly from the theoretical value of 2 which appears in these correlations. This problem is taken into account in the correlation used which is given by the following equation [41]:

$$D_{ax} = \frac{D_m}{\tau} + \frac{0.65 d_P (u/\varepsilon)}{\left(1 + 7\sqrt{\frac{D_m}{(d_P u/\varepsilon)}}\right)}, \tag{15}$$

which is valid for $Re < 100$ ($Re$ is about 70 for the four zeolites).

The initial and boundary conditions are similar to those of the first model. The total quantity adsorbed is the sum of the quantity at both types of site.

### 3.2.2. *Determination of parameters and numerical solution*

The two models contain a set of parameters available from experimental data and measurements. The two models are solved in the same way: the space variable is discretized in $N$ values. Each variable ($C$, $\bar{Q}$, $Q_s$, $C_s$ for the first model and $C$, $\overline{Q_i}$, $Q_{si}$, $C_{si}$, $\overline{Q_c}$, $Q_{sc}$, $C_{sc}$ for the second) is replaced by $N$ variables leading to a set of $4N$ variables for the first model and $7N$ variables for the second one. The mass-balance partial differential equation (Equation (3) or (11)) is then transformed into a system of $N$ ordinary differential equations (time) using finite differences of order 2 to represent the space derivatives. Each ordinary differential equation is replaced by a system of $N$ ordinary differential equations, and each algebraic equation is replaced by a system of $N$ algebraic equations. Then the global algebro-differential system (of $4N$ equations for the first model, $7N$ equations for the second model) was numerically solved using the ode15s function in MATLAB®.

The model parameters are determined by fitting the modelled results to the experimental data. An optimization procedure based on the Levenberg–Marquardt algorithm was used to fit the parameters to the experimental data. The following LS criterion is minimized:

$$LS = \sqrt{\frac{1}{n_{exp}}\sum_{j=1}^{n_{exp}}\frac{(Cout_{j,mod} - Cout_{j,exp})^2}{(Cout_{j,exp})^2}} \tag{16}$$

$n_{exp}$ is the number of experimental data and $C_{out}$ is the concentration of the TOL in the gas phase at the outlet of the fixed-bed.

The identified parameter of the first model is $k_p$. The identified parameters of the second model are: $k_{pi}$, $k_{pc}$.

### 3.2.3. *Results of the simulation*

As shown in Figure 4(a), the mathematical model with one site fitted well the experimental breakthrough of the three

Table 4. Adsorbed amounts and mass transfer coefficients.

| | $Q$ (mol kg$^{-1}$) | $Q_e$[a] (mol kg$^{-1}$) | $k_p$ ($\times$ 10$^4$ s$^{-1}$) | $k_c$[b] ($\times$ 10$^2$ m s$^{-1}$) |
|---|---|---|---|---|
| H-MOR | 0.66 | 0.67 | 5.8 | 5.9 |
| H-FAU | 1.22 | 1.18 | 1.7 | 5.9 |
| H-Z | 0.51 | 0.50 | see Table 5 | 6.2 |
| Na-Z | 0.53 | 0.51 | 2.1 | 6.0 |

[a]From isotherm models.
[b]$k_c$ Obtained from the relationship of Wakao and Funazkri: $(k_c\, d_p/D_m) = 2.0 + 1.1Re^{0.6}Sc^{0.3}$.

Table 5. Equilibrium parameters and mass transfer coefficients for the two site models.

| | $Q_{maxi}$ / $Q_{maxc}$ (mol kg$^{-1}$) | $b_i/b_c$ (m$^3$ mol$^{-1}$) | $k_{pi}$ ($\times$ 10$^4$ s$^{-1}$) | $k_{pc}$ ($\times$ 10$^4$ s$^{-1}$) | $k_c$ ($\times$ 10$^2$ m s$^{-1}$) |
|---|---|---|---|---|---|
| Parallel adsorption | 0.66 / 0.43 | 437 / 3.35 | **1.7** | **25.0** | 5.9 |
| Successive adsorption | 0.69 / 0.12 | 426 / 264 | **0.07** | **19.0** | 5.9 |
| | 0.69 / 0.12 | **162 / 307** | **1.1** | **16.0** | 5.9 |

Note: Identified values are in bold.

zeolites characterized by the isotherms well-described by the Langmuir model. However, among these three zeolites, the result for H-FAU was less accurate. The second model with two sites of adsorption also failed to represent the H-FAU breakthrough curve with good accuracy. Another model with one site of adsorption has been tested: the Thomas model.[24,25] It led to a slightly better representation suggesting that the adsorption kinetics might be taken into account, though it lacked accuracy in the intermediate zone of the breakthrough curve. This could be explained by the lack of precision of the isotherm modelling in the area of inlet concentration as mentioned earlier.

The adsorbed quantities and the parameters of the one site model are reported in Table 4. The quantities are close to those obtained at equilibrium and estimated using adsorption isotherms. It appears that the intrapellet mass transfer coefficients $k_p$ is greater for H-MOR than for Na-Z and H-FAU. The mass transfer depends on several parameters: hydrodynamics, the affinity between the adsorbent and adsorbate, the pore size and so on. The closer to one the ratio between the kinetic diameter of TOL and the pore size of zeolites is, the higher the affinity between the surface and the adsorbate, thanks to Van Der Walls forces. This ratio is lower for FAU (0.78) than for MOR (0.88). Thus, the breakthrough is steeper as observed for H-MOR. The size of the pore for TOL is similar in the case of H-Z and Na-Z (1.02), but the ratio is slightly higher than 1. In fact when the ratio is identical or slightly higher than 1, the transport of molecules is more difficult. These results are consistent with other studies.[42]

As far as H-Z is concerned, neither the first model with one site of adsorption nor the Thomas model described the profile of the experimental breakthrough curve of H-Z. Three breakthrough curves predicted by the second model are shown in Figure 4(b). First, the parameters $Q_{maxi}$, $Q_{maxc}$, $b_i$, $b_c$ of the DL model are used. Hence, a parallel adsorption is simulated, and internal mass transfer coefficient is determined for each site (reported in Table 5). As shown in Figure 4(b), this model does not fit well with the experimental data. Moreover, surprisingly, $k_{pc}$ is greater than $k_{pi}$ although the molecules that reach the sinusoidal channels have to pass through the straight channels and the intersections before being adsorbed in the sinusoidal channels. This result reinforces our conviction that adsorption at intersections and adsorption in sinusoidal channels takes place successively rather than simultaneously. In Figure 4(b), it can be seen that the use of the parameters of the SL model instead of the parameters of the DL model gives better results but fails to represent the end of the breakthrough curve. Indeed, since the model does not interconnect the two sites, it seems to us that the use of the parameters of the SL model could not be suitable, particularly $b_i$, because some of the molecules adsorbed at the intersections will migrate to the channels. So if it is only considered that the molecules finally stay at the intersections, the parameter $b_i$ would be lower. That is why in order to simulate the successive adsorptions, $b_i$ and $b_c$ have been identified together with $k_{pi}$ and $k_{pc}$. This simulation fits the experimental breakthrough curve very well, as shown in Figure 4(b). Initially, the adsorption of TOL occurs in the intersections of the framework and then continues inside the sinusoidal channels after a reorientation of the molecules adsorbed at the intersections. The global mass transfer then becomes more limiting leading to a change in the slope, which explains why the identified mass transfer coefficient for the intersections is lower for H-Z than for Na-Z (Table 4). Indeed, for Na-Z, the intersections are probably the only adsorption site, as reported before, and no change in diffusion rate can then be observed. The identified values of the parameters are reported in Table 5. It should be noted that $k_{pi}$ is lower than $k_{pc}$. Indeed, for intersections, intracrystalline diffusion is important since the molecules

move along the straight channels to reach the intersections. While for the sinusoidal channels, intracrystalline diffusion is lower since this adsorption results from a reorientation of the molecules already adsorbed at the intersections. It can also be seen that the value of $b_c$ is more-or-less the same as for the isotherm. However, the value of $b_i$ is much lower as expected and previously explained.

## 4. Conclusion

Thanks to the results of experimental and modelling studies, a better understanding of adsorption phenomena is proposed according to the nature of the zeolites.

(i) It is obvious that adsorption is dependent on the way the zeolites are structured. According to the size of the pores, TOL can enter easily into the network (FAU) or can only enter with difficulty (Mordenite or Na-Z). The Langmuir model fits these 'type I' isotherms with a good accuracy and the LDF approximation gives a good simulation of breakthrough curves for these three adsorptions.

(ii) However, some chemical phenomena can occur and change the adsorption characteristics. For example, with ZSM-5, the compensating cation can play a role. Because of some strong interactions, the solute can be blocked in one site of adsorption (in the case of Na-Z) whereas it can spread to a secondary internal network if no interaction occurs (in the case of H-Z).

(iii) In that latter case, two sites of adsorption are highlighted and two SL models fit the experimental isotherm much better than a DL model suggesting that adsorption on the two sites occur in series rather than in parallel.

(iv) In the case of the breakthrough curves, the development of a model is proposed, taking into account two different sites of adsorption, sinusoidal channels and intersections. This model fails to represent the breakthrough curve if parallel adsorption is assumed but can give a high level of accuracy with the hypothesis of successive adsorption.

## Nomenclature

| | |
|---|---|
| $a$ | specific area ($m^2\ m^{-3}$) |
| $b$ | Langmuir constant ($m^3\ mol^{-1}$) |
| $C$ | concentration of the TOL in the gas phase at the outlet of the fixed-bed ($mol\ m^{-3}$) |
| $C_s$ | gas concentration at the surface of the pellet ($mol\ m^{-3}$) |
| $C_e$ | equilibrium concentration in gas phase ($mol\ m^{-3}$) |
| $C_0$ | initial concentration ($mol\ m^{-3}$) |
| $C_{TOLin}$ | inlet concentration ($mol\ m^{-3}$) |
| $D_{ax}$ | axial dispersion coefficient ($m^2\ s^{-1}$) |
| $D_m$ | molecular diffusivity ($m^2\ s^{-1}$) |
| $d_p$ | particle diameter (m) |
| DL | Double Langmuir |
| $F$ | fluid flow ($m^3\ h^{-1}$) |
| $H$ | height of bed (m) |
| $k_c$ | external mass transfer coefficient ($m\ s^{-1}$) |
| $k_p$ | intrapellet mass transfer coefficient ($s^{-1}$) |
| $k_{pi}$ | intrapellet mass transfer coefficient in the first adsorption site for model 2 ($s^{-1}$) |
| $k_{pc}$ | intrapellet mass transfer coefficient in the second adsorption site for model 2 ($s^{-1}$) |
| LS | minimized criterion |
| $m$ | mass of zeolites (g) |
| $M$ | molecular weight ($g\ mol^{-1}$) |
| $N$ | number of discretization points |
| $n_{exp}$ | number of experimental data |
| $Q$ | adsorbed quantity of TOL ($mol\ kg^{-1}$) |
| $Q_e$ | moles of adsorbate adsorbed per unit mass of adsorbent at the equilibrium ($mol\ kg^{-1}$) |
| $\overline{Q_i}$ | mean adsorbed quantity in the first adsorption site for model 2 ($mol\ kg^{-1}$) |
| $\overline{Q_c}$ | mean adsorbed quantity in the second adsorption site for model 2 ($mol\ kg^{-1}$) |
| $\bar{Q}$ | mean adsorbed quantity in micropores ($mol\ kg^{-1}$) |
| $Q_{max}$ | Langmuir Parameter – maximum adsorbed quantity ($mol\ kg^{-1}$) |
| $Q_s$ | concentration adsorbed on at the surface of adsorbent ($mol\ kg^{-1}$) |
| SL | Successive Langmuir |
| $t$ | time (s) |
| $t_s$ | time needed to reach the saturation |
| $T$ | temperature (K) |
| $u$ | superficial velocity ($m\ s^{-1}$) |
| $V$ | volume of reactor (L) |
| $z$ | axial coordinate in the column (m) |
| $\epsilon$ | porosity of bed |
| $\rho$ | bed density ($kg\ m^{-3}$) |
| $\tau$ | tortuosity factor (about four for the four studied zeolites) |

### Dimensionless Numbers

| | |
|---|---|
| $Re$ | Reynolds number ($\rho u d_p/\mu$) |
| $Sc$ | Schmidt number ($\mu/\rho D_m$) |
| $Pe$ | Peclet number ($u d_p/\varepsilon D_m$) |


### Acknowledgements

N. Brodu gratefully acknowledges Mr. Khairul Nizam SAIFUL EMPON for his valuable collaboration.


### Disclosure statement

No potential conflict of interest was reported by the authors.

## Funding

This work was supported by the French Ministry of Higher Education and Research.

## References

[1] Agueda VI, Crittenden BD, Delgado JA, Tennison SR. Effect of channel geometry, degree of activation, relative humidity and temperature on the performance of binderless activated carbon monoliths in the removal of dichloromethane from air. Sep Purif Technol. 2011;78:154–163.

[2] Finne G, Vaesen S, Decroly A. Gas-phase adsorption of butan-1-ol: integrated procedure for assessing the performances of adsorbent materials. Récents Progrès en Génie des Procédés. 2011;101.

[3] Huang Z, Kang F, Liang K, Hao J. Breakthrough of methyethylketone and benzene vapors in activated carbon fiber beds. J Hazard Mater. 2003;98:107.

[4] Pires J, Carvalho A, De Carvalho M-B. Adsorption of volatile organic compounds in Y zeolites and pillared clays. Microporous Mesoporous Mater. 2001;43:277–87.

[5] Nevers N. Air pollution control engineering. Singapore: Mc-Graw-Hill; 2000.

[6] Guillemot M, Mijoin J, Mignard S, Magnoux P. Adsorption of tetrachloroethylene (PCE) in gas phase on zeolites of faujasite type: influence of water vapour and of Si/Al ratio. Microporous Mesoporous Mater. 2008;111:334.

[7] Dou B, Hu Q, Li J, Qiao S, Hao Z. Adsorption performance of VOCs in ordered mesoporous silicas with different pore structures and surface chemistry. J Hazard Mater. 2011;186:1615–1624.

[8] Boulinguiez B, Le Cloirec P. Adsorption on activated carbons of five selected volatile organic compounds present in biogas: comparison of granular and fiber cloth materials. Energy Fuels. 2010;24:4756–4765.

[9] Khan FK, Ghosal AK. Removal of volatile organic compounds from polluted air. J Loss Prevent Proc 2000;13: 527–545.

[10] Brodu N, Zaitan H, Manero M-H, Pic J-S. Removal of volatile organic compounds by heterogeneous ozonation on microporous synthetic alumino silicate. Water Sci Technol. 2012;66:2020–2026.

[11] Chica A, Strohmaier K, Iglesia E. Adsorption, desorption, and conversion of thiophene on H–ZSM5. Langmuir. 2004;20:10982–10991.

[12] Serrano DP, Calleja G, Botas JA, Gutierrez FJ. Characterization of adsorptive and hydrophobic properties of silicalite-1, ZSM-5, TS-1 and beta zeolites by TPD techniques. Sep Purif Technol. 2007;54:1–9.

[13] Serna-Guerrero R, Sayari A. Applications of pore-expanded mesoporous silica: adsorption of volatile organic compounds. Environ Sci Technol. 2007;41:4761–4766.

[14] Das D, Gaur V, Verma N. Removal of volatile organic compound by activated carbon fiber. Carbon. 2004;42:2949.

[15] Brosillon S, Manero M-H, Foussard J-N. Mass transfer in VOC adsorption on zeolite: experimental and theoretical breakthrough curves. Environ Sci Technol. 2001;35: 3571.

[16] Lee S-W, Cheon J-K, Park H-J, Lee M-G. Adsorption characteristics of binary vapors among acetone, MEK, benzene and toluene. Korean J Chem Eng. 2008;25:1154.

[17] Bhatia S, Abdullah AZ, Wong CT. Adsorption of butyl acetate in air over silver-loaded Y and ZSM-5 zeolites: experimental and modelling studies. J Hazard Mater. 2009;163:73.

[18] Monneyron P, Manero M-H, Foussard J-N. Measurement and modeling of single- and multi-component adsorption equilibria of VOC on high-silica zeolites. Environ Sci Technol. 2003;37:2410–2414.

[19] Dragoi B, Rakic V, Dumitriu E, Auroux A. Adsorption of organic pollutants over microporous solids investigated by microcalorimetry techniques. J Therm Anal Calorim. 2010;99:733.

[20] Kim K-J, Ahn H-G. The effect of pore structure of zeolite on the adsorption of VOCs and their desorption properties by microwave heating. Microporous Mesoporous Mater. 2012;152:78.

[21] Lucas S, Calvo MP, Palencia C, Cocero MJ. Mathematical model of supercritical CO2 adsorption on activated carbon – effect of operating conditions and adsorption scale-up. J Supercrit Fluids. 2004;32:193–201.

[22] Carrère H, Sochard S, Bascoul A, Wilhelm AM, Delmas H. Whey proteins extraction by fluidized ion exchange chromatography: isotherms determination and process modelling. Trans I ChemE, Part C Food Bioproducts Process. 1994;72:216–226.

[23] Carratala-Abril J, Lillo-Rodenas MA, Linares-Solano A, Cazorla-Amoros D. Activated carbon for the removal of low-concentration gaseous toluene at the semipilot scale. Ind Eng Chem Res. 2009;48:2066–2075.

[24] Hashim MA, Chu KH. Prediction of protein breakthrough behavior using simplified analytical solution. Sep Purif Technol. 2007;53:189–197.

[25] Réguer A, Sochard S, Hort C, Platel V. Measurement and modelling of adsorption equilibrium, adsorption kinetics and breakthrough curve of toluene at very low concentrations onto activated carbon. Environ Technol. 2011;32:757–766.

[26] Lorimier C, Subrenat A, Le Coq L, Le Cloirec P. Adsorption of toluene onto activated carbon fiber cloths and felts: application in indoor air treatment. Environ Technol. 2005;26:1217–1230.

[27] Tantet J, Eic M, Desai R. Breakthrough study of the adsorption and separation of sulphur dioxide from wet gas using hydrophobic zeolites. Gas Sep Purif. 1995;9:213–220.

[28] Tien C. Adsorption calculations and modeling. Boston: Butterworth-Heinemann; 1994.

[29] Lesage G, Sperandio M, Tiruta-Barna L. Analysis and modelling of non-equilibrium sorption of aromatic micropollutants on GAC with a multi-compartment dynamic model. Chem Eng J. 2010;160:457.

[30] Ding LP, Bhatia SK, Liu F. Kinetics of adsorption on activated carbon: application of heterogeneous vacancy solution theory. Chem Eng Sci. 2002;57:3909–3928.

[31] Breck DW. Zeolite molecular sieves: structure, chemistry and use. New York: Wiley; 1974.

[32] Brunauer S, Emmett PH, Teller E. Adsorption of gases in multimolecular layers. J Am Chem Soc. 2002;60:309–319.

[33] Horvath G, Kawazoe K. Method for the calculation of effective pore size distribution inn molecular sieve. J Chem Eng Jpn. 1983;16:470.

[34] Song L, Sun Z, Duan L, Gui J, McDougall GS. Adsorption and diffusion properties of hydrocarbons in zeolites. Microporous Mesoporous Mater. 2007;104:115.

[35] Wang F, Wang W, Huang S, Teng J, Xie Z. Experiment and modeling of pure and binary adsorption of n-butane and butane-1 on ZSM-5 zeolites with different Si/Al ratios. Chin J Chem Eng. 2007;15:376–386.

[36] Szabelski P, Narkiewicz-Michalek J, Rudzinski W. Coverage dependence of aromatic hydrocarbon diffusion in silicalite: predictions of the three-site lattice model. Appl Surf Sci. 2002;196:191–201.

[37] Serra RM, Miro EE, Bolcatto P, Boix AV. Experimental and theoretical studies about the adsorption of toluene on

ZSM5 and mordenite zeolites modified with Cs. Microporous Mesoporous Mater. 2012;147:17–29.
[38] Zhang W, Qu Z, Li X, Wang Y, Ma D, Wu J. Comparison of dynamic adsorption/desorption characteristics of toluene on different porous materials. J Environ Sci. 2012;24:520.
[39] Wakao N, Funazkri T. Effect of fluid dispersion coefficients on particle-to-fluid mass transfer coefficients in packed beds. Chem Eng Sci. 1978;33:1375–1384.
[40] Yang RT. Gas separation by adsorption processes. London: Imperial College Press; 1997.
[41] Delgado JMPQ. Longitudinal and transverse dispersion in porous media. Tran IChemE Part A, Chem Eng Res Des. 2007;85:1245–1252.
[42] Meininghaus CKW, Prins R. Sorption of volatile organic compounds on hydrophobic zeolites. Microporous Mesoporous Mater. 2000;35–36:349–365.